Cellulose (2017) 24:4773–4784
DOI 10.1007/s10570-017-1455-y

ORIGINAL PAPER

Poly(lactic acid)-based biocomposites reinforced with modified cellulose nanocrystals

Yuanyuan Yin · Lina Zhao · Xue Jiang · Hongbo Wang · Weidong Gao

Received: 7 May 2017 / Accepted: 12 August 2017 / Published online: 24 August 2017

Abstract This work investigates reinforcing poly(lactic acid) (PLA) nanocomposites using triazine derivative-grafted cellulose nanocrystals (CNCs). A hydrophobic triazine derivative was synthesized and applied to modify CNCs to improve their thermal stability and diminish the hydrophilicity of the nanoparticles. CNCs before and after modification were used to reinforce PLA nanocomposites by a hot compression process. The results of thermogravimetric analysis indicated that the initial thermal decomposition temperature of modified nanocrystals was improved by approximately 100 °C compared to the original CNCs. That is, the thermal stability of modified cellulose nanocrystals was improved due to the shielding effect of CNCs by a hydrophobic aliphatic amine layer on the surface of the nanoparticles. The results of dynamic contact angle measurements revealed a decrease of hydrophilicity of the modified CNCs. The results from scanning electron microscopy and a UV–Vis spectrophotometer revealed that the compatibility between the modified nanocrystals and the PLA was improved. Finally, the results of tensile tests indicated a significant improvement in terms of breaking strength and elongation at the break point.

Keywords Cellulose nanocrystals · Triazine derivative · Thermal stability · Compatibility · Poly(lactic acid) nanocomposites

Y. Yin · X. Jiang (✉) · H. Wang (✉) · W. Gao
Jiangsu Engineering and Technology Research Center for Functional Textiles, Jiangnan University, Wuxi 214122, Jiangsu, China
e-mail: jiangx@jiangnan.edu.cn

H. Wang
e-mail: wxwanghb@163.com

Y. Yin · L. Zhao · X. Jiang · H. Wang · W. Gao
Key Laboratory of Eco-textiles of Ministry of Education, Jiangnan University, Wuxi 214122, Jiangsu, China

Introduction

In the last few years, biodegradable composites have been investigated and considered as an ideal type of product in order to replace nondegradable petroleum-based materials (Jonoobi et al. 2010; Kowalczyk et al. 2011; Zhang et al. 2015). Polylactic acid (PLA) is one of the most suitable matrix materials for such biocomposites because of its relatively low cost, biocompatibility, processibility, and eco-friendly nature (Rasal et al. 2010; Singhvi and Gokhale 2013; Arrieta et al. 2014; Fortunati et al. 2015; Zhang et al. 2015). However, it has some drawbacks, which limit its use in certain applications (Yu et al. 2010; Yee et al. 2016). Although its tensile strength and elastic modulus are comparable to poly(ethylene terephthalate), one major disadvantage of PLA is its brittleness (Nakagaito et al. 2009; Rasal and Hirt 2009). Therefore, it is essential to find appropriate fillers to increase

the toughness of PLA materials in order to expand their application.

Cellulose nanocrystals (CNCs) have aroused much attention due to their biocompatibility, biodegradability, light weight, nano-scale effects, low cost, high specific strength and modulus (138 GPa of Young's modulus and 1.7 GPa of tensile strength), unique morphology, and relatively reactive surface (Azouz et al. 2012; Lin et al. 2012; Habibi et al. 2008; Liu et al. 2015). They have been widely studied as reinforcing agents in different kinds of nanocomposites, such as poly(ε-caprolactone) (Zoppe et al. 2009; Lonnberg et al. 2011; Mi et al. 2014; Stroganov et al. 2015), PLA (Goffin et al. 2011; Salmieri et al. 2014; Kamal and Khoshkava 2015; Bagheriasl et al. 2016), and polystyrene (PS) (Wang et al. 2008; Zhang et al. 2013; Huan et al. 2015), etc. The preparation of CNCs based on sulfuric acid hydrolysis is considered to be the most mainstream approach. Negatively charged sulfate esters are introduced on the surface of the obtained CNCs when using sulfuric acid as a hydrolyzing agent. The charged sulfate esters can promote the dispersion of the CNCs in water because like charges repel each other. However, the thermal stability of the nanoparticles is diminished by the sulfate esters, which is attributed to their catalytic nature (Roman and Winter 2004; Abraham et al. 2016). The inferior thermal stability of CNCs limits its use because most polymeric composites are processed at temperatures close to 200 °C or above (Lin and Dufresne 2013). In addition, CNCs present obvious hydrophilicity because of a large amount of hydroxyl groups on their surface, which limits the compatibility between hydrophilic CNCs and a hydrophobic polymeric matrix (Habibi et al. 2010; Bagheriasl et al. 2015; Morelli et al. 2016). Therefore, there are two challenges to overcome in the preparation of nanocomposites reinforced by CNCs: the inferior thermal stability and the poor compatibility with nonpolar materials.

There are a large number of reactive hydroxyl groups on the surface of CNCs, which can react with different active groups, such as carboxyl, epoxy, and siloxane, etc. In order to improve the thermal stability and hydrophobicity of CNCs, different chemical and physical modification strategies have been attempted (Eyley and Thielemans 2014), such as solubilization using a third component as compatibilizer (Pracella et al. 2014; M-UI Haque et al. 2017), esterification (Braun and Dorgan 2009; Sobkowicz et al. 2009), oxidation (Shimizu et al. 2013, 2014a, b), polymer grafting (Ljungberg et al. 2005; Roy et al. 2005; Morandi et al. 2009; Goffin et al. 2012), etc. The resulting nanocrystals show good dispersion abilities in organic solvents and excellent thermal stability. The goal of these methods was to introduce hydrophobic groups on the surface of the CNCs to replace the hydrophilic hydroxyl groups.

Triazine is an important intermediate in the dye and pharmaceutical industries. There are three reactive chlorine groups in the chemical structure of 2,4,6-trichloro-1,3,5-triazine (TCT). In this study, a triazine derivative was synthesized through the reaction between TCT and hexylamine (HA), and then the derivative was introduced on the surface of the CNCs. As shown in Scheme 1, one of the chlorine groups reacted with the hydroxyl groups on the surface of the CNCs, and the second chlorine groups reacted with the amino groups of aliphatic amine. The hydrophilicity of the nanoparticals was diminished and the thermal stability of the CNCs was improved because of the hydrophobic aliphatic chains covering their surface.

Experimental

Materials

Cotton, hydrochloric acid, sulfuric acid, acetone, toluene, tetrahydrofuran (THF), sodium hydroxide (NaOH), sodium bicarbonate and HA were purchased from Sinopharm Chemical Reagent; TCT was obtained from TCI Shanghai; hexylamine was supplied by J&K Scientific; and PLA with $M_w = 100{,}000$ g/mol was provided by Shanghai Yisheng Industry.

Preparation of cellulose nanocrystals

According to our previous article (Yin et al. 2016), cellulose nanocrystals were fabricated from cotton using sulfuric acid hydrolysis. In brief, about 10 g of cotton was mixed with 200 mL of sulfuric acid aqueous solution (64 wt%) in a three-neck flask, which was equipped with a stirrer, thermometer and condenser. The reactive mixture was stirred for 1 h at 45 °C for hydrolysis, then about 200 mL of cold water (about 0 °C) was poured into the obtained suspension

Scheme 1 The modification of CNCs using TCT and aliphatic amine

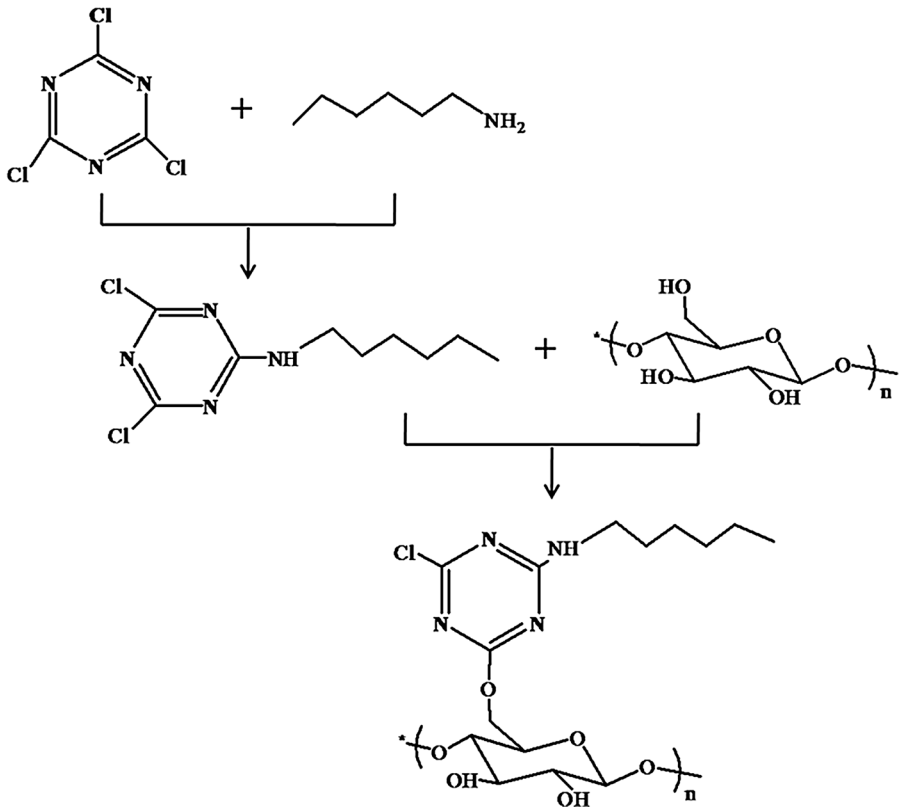

to stop the reaction. Subsequently, the suspension was centrifuged at 10,000 rpm until it had no obvious stratification and existed as a kind of homogeneous suspension. The CNCs powders were received after dialysis against deionized water until the pH of the water reached a value of 7.0 and after freeze-drying.

Synthesis of triazine derivative

The triazine derivative was synthesized as follows: first, 7.38 g of triazine and a balanced amount of acetone were added to a 250-mL three-neck round-bottom flask. Then, 4.86 g of HA was added dropwise into the above solution and the reaction was carried out at 0–5 °C for 8 h. The pH of the solution was adjusted to around 10 using 10 wt% NaOH solution. Finally, the triazine derivative, which has been named TCT–HA, was obtained after the solution was filtered, washed with 0.1 mol/L hydrochloric acid, 0.1 mol/L sodium bicarbonate and distilled water, and recrystallized using toluene (Pearlman and Banks 1948). ^{13}C NMR: (153.19, 150.76, 148.94, triazine part), (14.76, 23.32, 26.81, 29.77, 32.34, 45.70, HA portion).

Modification of cellulose nanocrystals with triazine derivative

The grafting reaction of the TCT–HA onto cellulose nanocrystals was performed as follows: Briefly, 0.5 g of CNCs was swollen in NaOH solution in a 100-mL three-neck round-bottom flask and stirred at pH = 10 for 30 min. Then, 0.690 g of TCT–HA dissolved in THF was added dropwise into the flask and the reaction was performed at 40 °C for 4 h. The triazine derivative-grafted cellulose nanocrystals (CNC–TCT–HA) was obtained after the solution was filtered, washed with THF using Soxhlet extraction, washed with distilled water and freeze-dried.

Preparation of nanocomposites

PLA nanocomposites reinforced with pure and modified CNCs were fabricated by hot compression. The process was carried out at 170 °C for 10 min under 40 MPa pressure. The PLA matrix and CNCs were pre-mixed by dry mixing the powders of the components. Then, the mixed powders were transferred into

molds followed by hot-pressing. CNCs before and after modification were utilized to reinforce the PLA matrix, which were marked as PLA/CNC and PLA/CNC–TCT–HA, respectively. The loading levels of CNC–TCT–HA by weight of the PLA matrix were 1, 2, 3, 4 and 5 wt%.

Characterization

Transmission electron microscopy (TEM) was performed on a JEM-2100 electron microscope operating at an acceleration voltage of 80 kV to characterize the morphology and distribution of the cellulose nanocrystals. A drop (5 μL) of a diluted suspension of CNCs was deposited on a copper grid and then stained with phosphotungstic acid (1 wt%) to improve the contrast.

The synthesis of the TCT derivative and the modification of the CNCs were characterized by a Bruker 400 M, colid-state ^{13}C NMR, and Fourier transform infrared spectroscopy (FT-IR). The samples were prepared by the KBr pellet method. The resolution of the spectrometer was 4 cm^{-1}, the wave number range was 400–4000 cm^{-1}, and the samples were scanned 30 times.

The grafting efficiency (GE%) of TCT–HA grafted on the surface of CNCs was determined using a Quanta 200 (FEI) electron microscope equipped with an energy dispersive X-ray (EDX) system. The carbon, oxygen, sulfur, nitrogen and chlorine elements content of CNC–TCT–HA were measured. The GE% was calculated according to Eq 1:

$$\mathrm{GE\%}\ \cdot C_{\mathrm{TCT-HA}} + (1 - \mathrm{GE\%}\ ) \cdot C_{\mathrm{CNC}} = C_{\mathrm{CNC-TCT-HA}} \quad (1)$$

where C is the relative nitrogen content of the sample.

The thermal degradation of the CNCs was analyzed using a thermal analyzer TGA/SDTA851e under nitrogen flow. About 5 mg of dried samples were heated from 30 to 600 °C at a heating rate of 10 °C/min.

Contact angle measurement was performed to investigate the hydrophilicity of the CNCs before and after modification, which was performed at room temperature using a DSA25S-Kruss contact angle measuring device. CNCs before and after modification were compacted under 20 MPa to obtain samples with smooth surfaces. A small drop of water (2 μL) was placed on the surface of the samples. Then, the contact angle was calculated using a sessile drop contact angle system.

The homogeneity of the PLA composites was observed using scanning electron microscopy (SEM) (su1510 device; Hitachi Zosen) at 30 kV. The transmittance of the nanocomposite films was measured using a UV–Vis spectrophotometer at wavelengths from 400 to 800 nm. The morphology of the PLA composites was further studied using atomic force microscopy (AFM) from Bruker. The equipment was operated in tapping mode in air at room temperature with a scan rate of 1 Hz and a scan angle of 0°. Thin sections of the PLA composites were obtained using a cryo-ultramicrotome. The topography, amplitude and phase images were all recorded simultaneously.

Thermostable PS composites were analyzed by a differential scanning calorimeter (DSC). In order to eliminate thermal history, the samples were scanned from 30 to 200 °C at a heating rate of 10 °C/min, and maintained at 200 °C for 5 min, then cooled to 30 °C at a rate of 20 °C/min and maintained for 5 min. Finally, the samples were scanned from 30 to 200 °C at a heating rate of 10 °C/min.

The mechanical properties of the PLA composites were investigated through tensile measurements using a universal material experiment machine. The samples were thin rectangular films with dimensions of about 100 × 20 × 0.5 mm. The drawing speed was 2 mm/min. The drawing experiments were carried out 5 times for each sample in order to to avoid the inherent uncertainty in the tensile testing experiments for the thin samples used in the research.

Results and discussion

As shown in Fig. 1, TEM was performed to observe the morphology and dimensions of the cellulose nanocrystals. Rod-like nanoparticles were separated

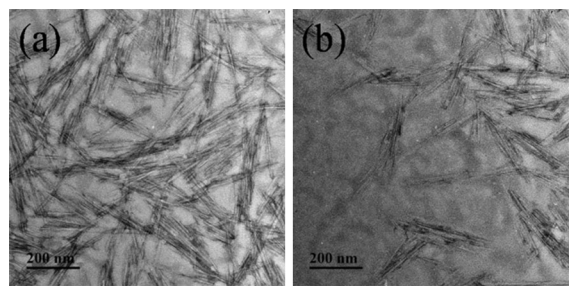

Fig. 1 TEM images of **a** CNCs; and **b** CNC–TCT–HA

from cotton using sulfuric acid hydrolysis. The size of the nanoparticles was about 200 nm in length and about 10 nm in width, which corresponds with the previous literature (Lin et al. 2012). According to the TEM images, agglomerations of nanoparticles were obvious because of the hydrogen bonding formed between the hydroxyl groups on the surface of the CNCs. Compared with the original CNCs, agglomeration of the TCT–HA-grafted CNCs was significantly decreased. It is worth nothing that the morphology of the modified CNCs was not seriously destroyed.

FT-IR was performed to analyze the synthesis of the triazine derivative and the chemical grafting of the CNCs. As shown in Fig. 2a, b, compared with TCT, the spectrum of the triazine derivative displayed the characteristic absorption bands of the -NH stretching at 3256 cm^{-1}, bands C=N at 1561 cm^{-1} and 1410 cm^{-1}, and C–Cl stretching at 798 cm^{-1}, corresponding to the absorption peaks of triazine. The presence of HA was proved by the $–CH_2$ and $–CH_3$ framework stretching at 2926 and 2854 cm^{-1}. ^{13}C NMR was recorded to further analyze the chemical structure of TCT–HA (Fig. 3). The signals at 153.19, 150.76, 148.94 ppm corresponded to triazine, while the signals at $\delta = 14.76$, 23.32, 26.81, 29.77, 32.34, and 45.70 ppm were assigned to the carbons on the hexylamine at C1, C2, C3, C4, C5 and C6, respectively. This indicated the successful synthesis of the triazine derivative.

Figure 2c, d presents the FT-IR spectra of CNCs and TCT–HA-grafted CNCs. The spectrum of TCT–HA-grafted CNCs not only showed all of the characteristic absorption peaks of CNCs, but also presented

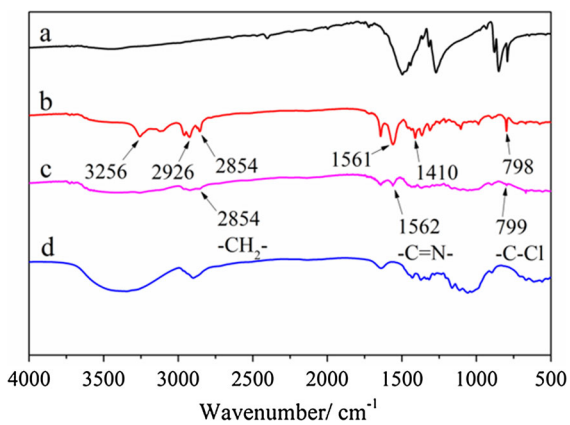

Fig. 2 FT-IR spectra of **a** TCT; **b** TCT-HA; **c** CNC–TCT–HA; and **d** CNCs

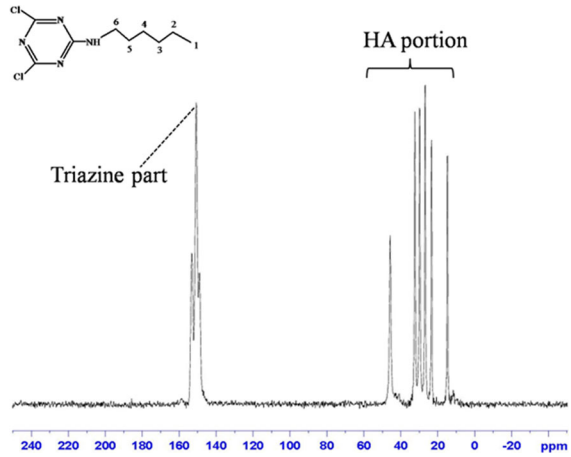

Fig. 3 ^{13}C NMR spectra of TCT–BA

the absorption bands of TCT–HA, such as $–CH_2$ stretching located at 2854 cm^{-1}, C=N stretching at 1562 cm^{-1} and C–Cl stretching situated at 799 cm^{-1}. This revealed that the CNCs were successfully grafted with TCT–HA. The successful grafting of TCT–HA on the CNCs surface was further proven using ^{13}C NMR, as shown in Fig. 4. The signals at $\delta = 105.83$, 71.50, 73.03, 75.20, 89.21 and 65.33 ppm were assigned to the carbons on the glucose ring at C1, C2, C3, C4, C5 and C6, respectively. The signals at 152.52 and 150.22 ppm corresponded to triazine. The ^{13}C NMR spectrum of CNC-g-PSt also showed signals at $\delta = 14.35$, 22.67, 26.51, 29.29, 31.91, and 45.31 ppm corresponding to the carbons on the HA at C10, C11, C12, C13, C14 and C15, respectively. This indicated that the CNCs surface was successfully grafted by the triazine derivative. Figure 5 shows the

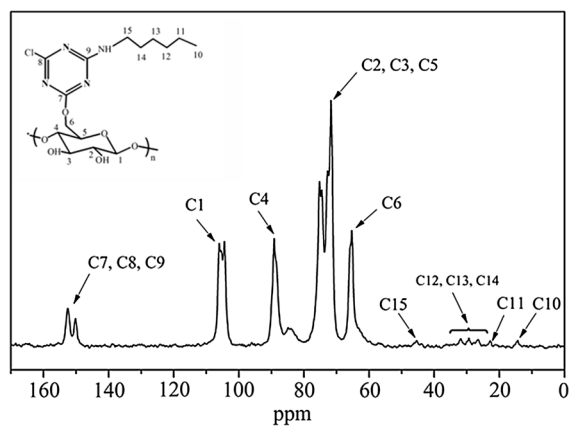

Fig. 4 ^{13}C NMR spectra of CNC–TCT–BA

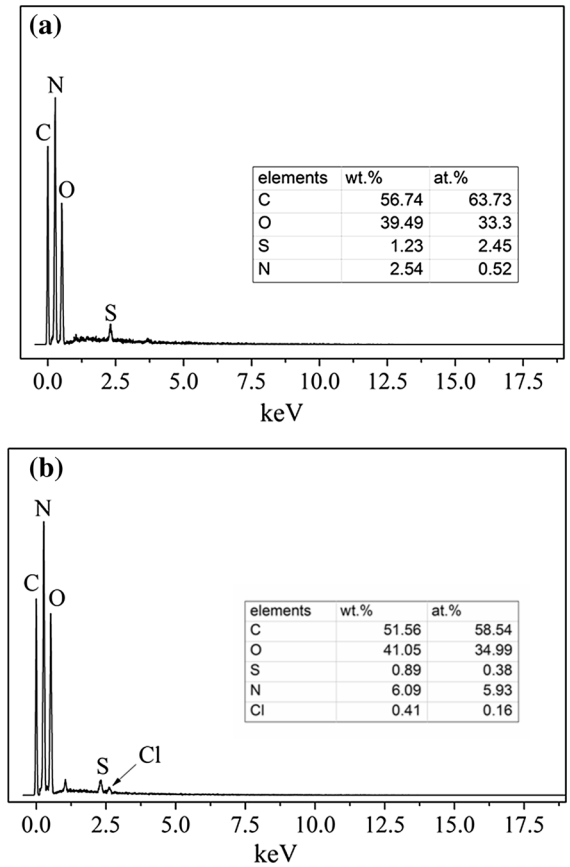

Fig. 5 EDX spectra of **a** CNCs; and **b** CNC–TCT–HA

element composition of pure CNCs and CNCs modified by TCT–HA. According to Eq. 1, the GE% of TCT–HA grafted on the surface of CNCs was 12.28%.

Figure 6 presents the thermal stability of CNCs before and after modification. It is obvious that the

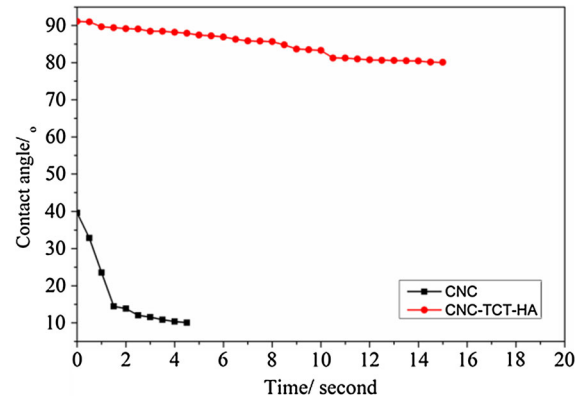

Fig. 7 Dynamic contact angle curves of CNCs and CNCs modified by TCT-HA

original CNCs presented a stepwise degradation behavior, which involved three processes. This corresponds with the previous literature (Roman and Winter 2004). The degradation processes started below 100 °C for both of the samples were attributed to the evaporation of adsorbed water. The degradation of the original CNCs between 200 and 400 °C presented two processes. The lower temperature degradation process corresponds to the degradation of the amorphous regions, where the material is more accessible and more highly sulfated, whereas the higher temperature degradation process relates to the breakdown of the unsulfated crystalline interior. Compared with the unmodified CNCs, the thermal stability of the CNCs modified with TCT–HA was significantly improved at about 100 °C because of the shielding effect of the sulfate groups.

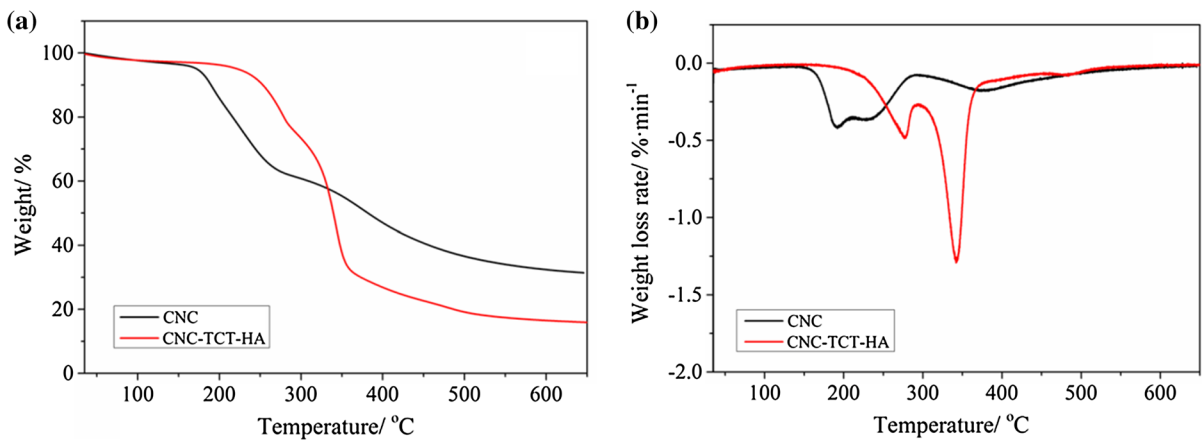

Fig. 6 **a** Curves of TGA of CNCs and CNC–TCT–HA; **b** DTG curves of CNCs and CNC–TCT–HA

In order to analyze the hydrophilicity of the CNCs before and after modification, contact angle measurements were performed, as shown in Fig. 7. It is clear that the CNCs presented a hydrophilic character, which led to inferior compatibility between the CNCs and the polymeric matrix. The contact angle of the modified CNCs was increased by approximately 50°. This result revealed that the nanoparticles modified with TCT–HA became more hydrophobic than the original CNCs, which was attributed to the hydrophobic hexylamine chains on the surface of the CNCs.

SEM of the fracture surfaces of the composites further revealed the compatibility between the CNCs and the polymeric matrix. As shown in Fig. 8, serious heterogeneity was observed in all samples with unmodified CNCs because of their aggregation. Black

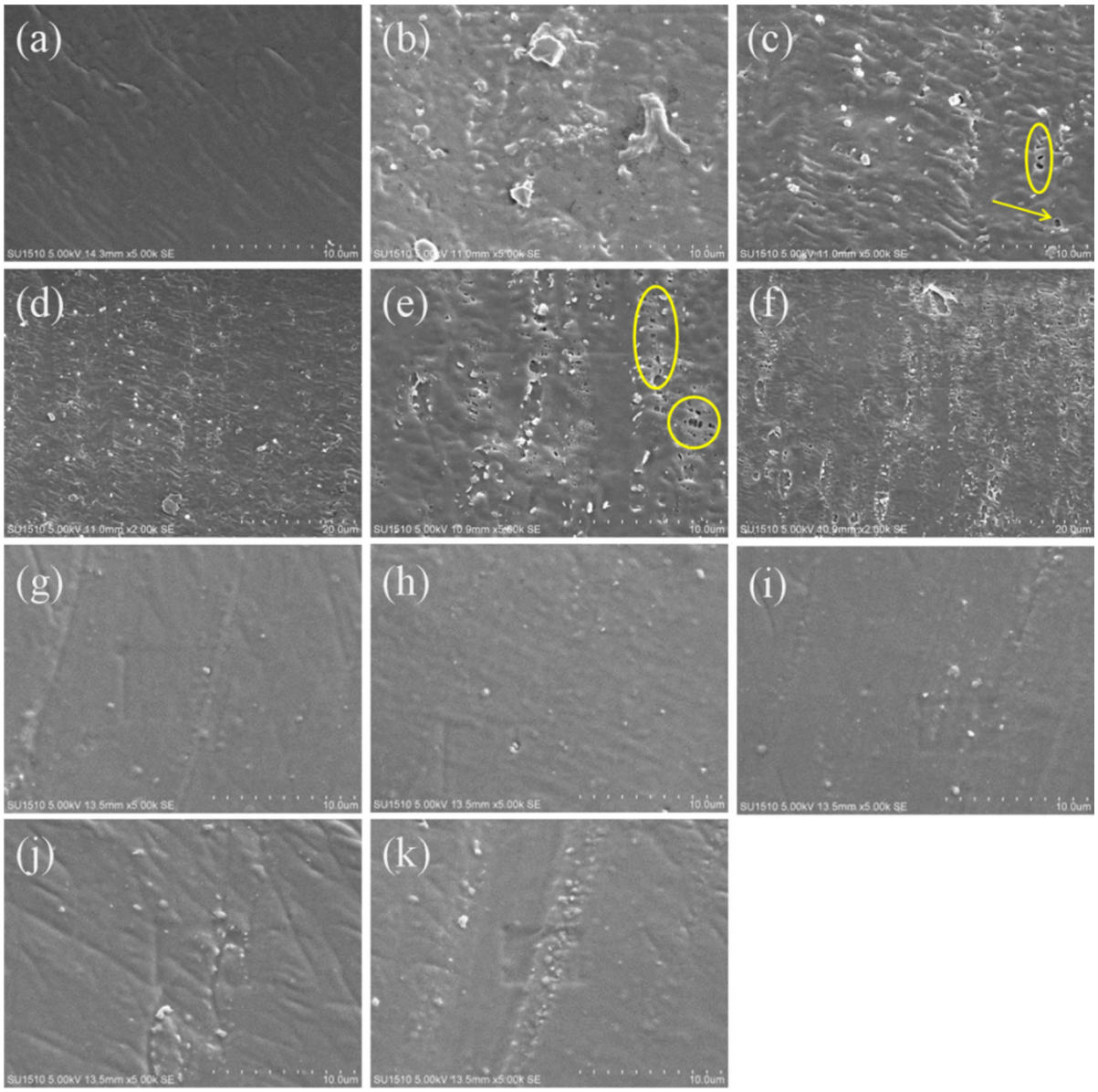

Fig. 8 SEM images for **a** PLA; **b** PLA/1% CNC; **c** PLA/2% CNC; **d** PLA/3% CNC; **e** PLA/4% CNC; **f** PLA/5% CNC; **g** PLA/1% CNC–TCT–HA; **h** PLA/2% CNC–TCT–HA; **i** PLA/3% CNC–TCT–HA; **j** PLA/4% CNC–TCT–HA; **k** PLA/5% CNC–TCT–HA

spots (indicated by a yellow arrow and circles in Fig. 8c, e) appeared in the composites with unmodified CNCs, which was attributed to the carbonization and degradation of the nanocrystals during the hot-pressing. Significantly, no black spots were observed in the PLA composites reinforced with the modified CNCs, which revealed the improved thermal stability of the modified CNCs corresponding to the results of TGA. Compared with the composites with unmodified CNCs, the modified CNCs dispersed homogeneously in the PLA matrix when the addition of nanoparticles was less than 3 wt%. The SEM images demonstrated a heterogeneous dispersion (white blocks in Fig. 8d–f) of nanoparticles when the additions of CNCs were more than 3 wt% because of the aggregation of the CNCs. To further reveal the dispersion of the modified CNCs in the PLA matrix, the morphology of the PLA composites reinforced with TCT–HA-grafted CNCs was recorded using AFM, as shown in Fig. 9. The topography, phase and amplitude of PLA/2%TCT–HA–CNC were all recorded simultaneously. The modified nanoparticles were 178 nm in length, which corresponded to the results of the TEM examination (Fig. 1). AFM images of PLA/TCT–HA–CNC also revealed the slight agglomerations at the surface of the PLA composites, corresponding to the SEM images. Although slight heterogeneities were present in the samples with 1 and 2% CNCs, the properties of the omposites were not seriously affected because of the uniform dispersion and low filler content.

UV–Vis transmittance spectra of the pure PLA and PLA composites reinforced with modified CNCs are shown in Fig. 10. The transmittance of the PLA composites declined sharply with the addition of pure CNCs, which was attributed to their aggregation and thermal degradation. Compared with PLA/CNC, the transmittance of PLA reinforced with TCT–HA-modified CNCs was maintained above 50% when the nanoparticle addition was less than 2 wt%, which indicated that the modified nanopartices dispersed in the PLA matrix homogeneously. These results corresponded to the SEM images.

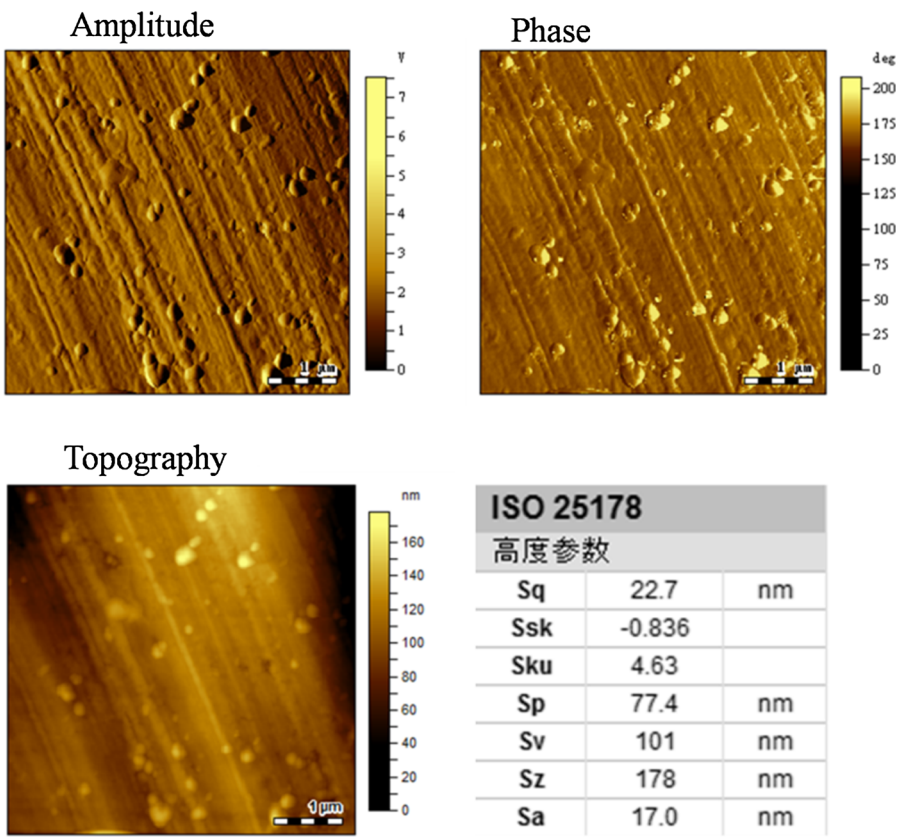

Fig. 9 AFM images of thin sections of PLA/2%TCT–HA–CNC composites

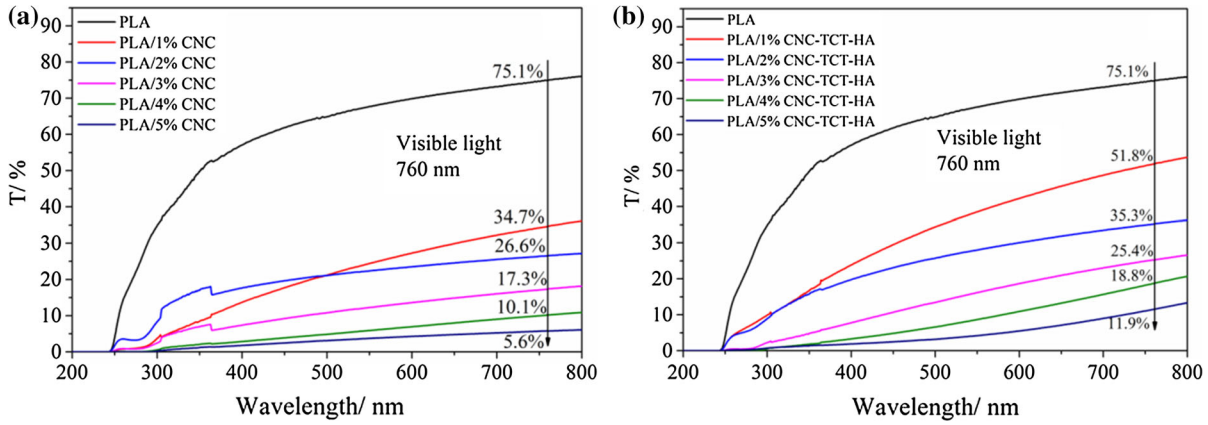

Fig. 10 Transmittance curves for **a** PLA/CNC and **b** PLA/CNC–TCT–HA

DSC was performed to analyze the thermal properties of the PLA composites after their preparation through hot-pressing. The effect of interactions between the nanofillers and the PLA, and the dispersion of CNCs in the matrix can be indicated using DSC. As shown in Fig. 11, the glass transition temperature (T_g) of the composites decreased with the introduction of the CNCs, a result ascribed to the

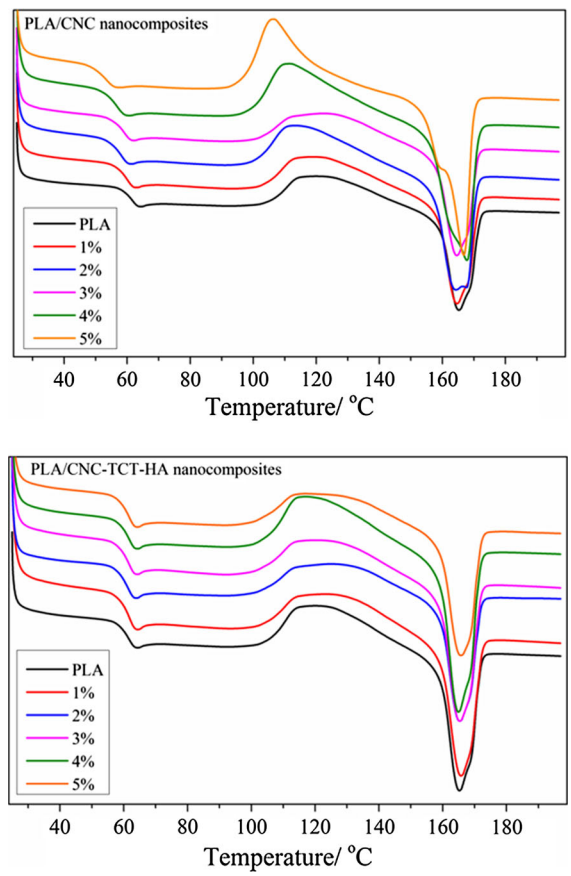

Fig. 11 DSC curves of PLA/CNC and PLA/CNC–TCT–HA composites

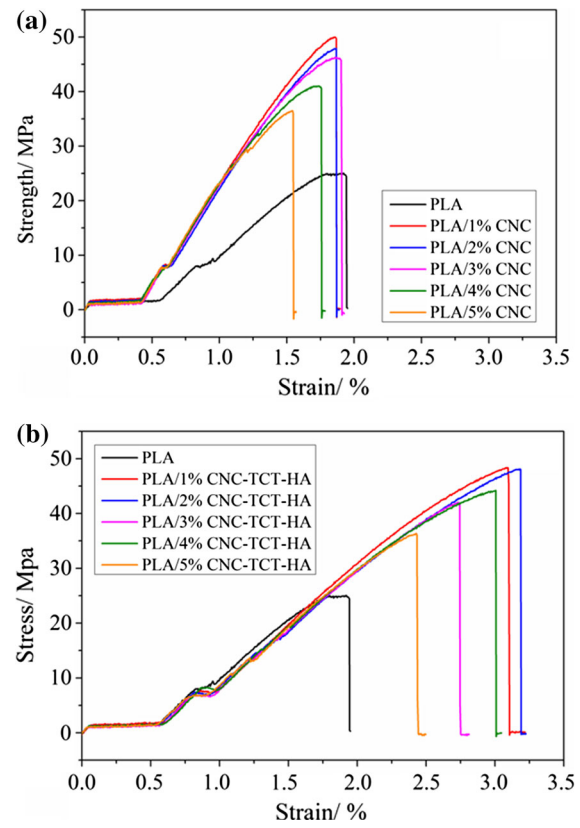

Fig. 12 Mechanical properties in terms of breaking strength and elongation at the break point for **a** PLA/CNC and **b** PLA/CNC–TCT–HA

Table 1 Tensile properties of the PLA matrix and PLA composites with CNCs before and after modification

Sample	Stress at break (MPa)	Elongation at break (%) (MPa)
PLA	25.06 ± 2.4	1.93 ± 0.6
PLA/1% CNC	49.98 ± 1.8	1.90 ± 0.4
PLA/2% CNC	47.92 ± 1.4	1.89 ± 0.3
PLA/3% CNC	46.26 ± 1.3	1.93 ± 0.5
PLA/4% CNC	41.00 ± 1.7	1.79 ± 0.4
PLA/5% CNC	36.49 ± 2.5	1.57 ± 0.6
PLA/1% CNC-TCT-HA	48.28 ± 0.9	3.10 ± 0.5
PLA/2% CNC–TCT–HA	48.06 ± 1.2	3.19 ± 0.7
PLA/3% CNC–TCT–HA	41.90 ± 1.8	2.74 ± 0.5
PLA/4% CNC–TCT–HA	44.07 ± 1.6	3.00 ± 0.6
PLA/5% CNC–TCT–HA	36.11 ± 2.4	2.43 ± 0.7

incompatibility and weak interfacial interaction between the nanoparticles and the PLA matrix. Compared with PLA/CNC, the T_g of composites reinforced with TCT–HA-grafted CNCs was almost the same as that of the PLA matrix. It is obvious that the cold crystallization temperature (T_{cc}) of PLA/CNC was lower than those of the PLA/CNC–TCT–HA composite, indicating that the unmodified CNCs acting as nucleating agents induced faster crystallization of the PLA. Double melting peaks were observed for the PLA/2%CNC and PLA/5%CNC composites, which was attributed to the imperfections in the crystals formed when the nuclei density was high, which occasioned the melting and re-crystallization of the imperfect crystals. For PLA/CNC–TCT–HA, the T_g and T_{cc} were maintained and no double melting peaks were seen, which indicated the good compatibility between the PLA matrix and the CNCs nanofillers.

As shown in Fig. 12, mechanical properties in terms of breaking strength and elongation at the break point were examined to reveal the reinforcement of the modified CNCs for the PLA composites. The values of all measured tensile properties are listed in Table 1, from which it can be seen that the pure PLA matrix had fragile properties, which limits its application in many fields. The breaking strength of the PLA composites increased with the addition of unmodified CNCs, which was attributed to their intrinsic mechanical properties. The elongation at the break point of PLA/CNC decreased because of the inferior compatibility between the PLA matrix and the unmodified CNCs. Compared with the pure PLA matrix and PLA/CNC, the breaking strength and elongation at the break point of the PLA composites reinforced with modified CNCs were improved, which was ascribed to the interfacial interaction between the PLA and the nanoparticles. However, it is worth nothing that the improvement of mechanical properties was weakened when the addition of CNCs was over 3 wt% because of the stress concentration on the interface between the CNCs and the PLA matrix. The compatibility between the TCT–HA-grafted CNCs and the polymeric matrix was improved in comparison with the unmodified CNCs. The results of tensile measurements revealed that the mechanical properties of the PLA composites reinforced with TCT–HA-grafted CNCs were improved to some extent.

Conclusions

A triazine derivative was successfully synthesized and innovatively grafted onto the surface of cellulose nanocrystals. The thermal stability of the modified CNCs was improved by 100 °C and the hydrophilicity of the modified nanoparticles declined at the same time. Compared with pure CNCs, the modified nanoparticles dispersed in the PLA matrix homogeneously. Therefore, the thermal properties of the PLA composites reinforced with the modified CNCs were improved and the transmittance of the PLA/CNC–TCT–HA composites was maintained. The results of tensile measurements revealed that the mechanical properties of the PLA composites reinforced with TCT–HA-grafted CNCs were improved. Nevertheless, a better result may be achieved by using a fatty amine with longer molecular chains to synthesis the

TCT derivative and to modify CNCs, and all these studies will be presented in the future work.

Acknowledgments The authors are grateful to the National Natural Science Foundation of China (Grant No. 31570578 and 31270632), the Fundamental Research Funds for the Central Universities (Grant No. JUSRP51622A), the Graduate Student Innovation Plan of the Jiangsu Province of China (KYLX16_0790) and the fund supported by China Scholarship Council.

References

Abraham E, Kam D, Nevo Y, Slattegard R, Rivkin A, Lapidot S, Shoseyov O (2016) Highly modified cellulose nanocrystals and formation of epoxy-nanocrystalline cellulose (CNC) nanocomposites. ACS Appl Mater Interfaces 8(41):28086–28095

Arrieta MP, Fortunati E, Dominici F, Rayon E, Lopez J, Kenny JM (2014) Multifunctional PLA-PHB/cellulose nanocrystal films: processing, structural and thermal properties. Carbohydr Polym 107(8):16–24

Azouz KB, Ramires EC, Fonteyne WV, Kissi NE, Dufresne A (2012) Simple method for the melt extrusion of a cellulose nanocrystal reinforced hydrophobic polymer. Acs Macro Lett 1(1):236–240

Bagheriasl D, Carreau PJ, Dubois C, Riedl B (2015) Properties of polypropylene and polypropylene/poly(ethylene-co-vinyl alcohol) blend/CNC nanocomposites. Compos Sci Technol 117:357–363

Bagheriasl D, Carreau PJ, Riedl B, Dubois C, Hamad WY (2016) Shear rheology of polylactide (PLA)–cellulose nanocrystal (CNC) nanocomposites. Cellulose 23:1885–1897

Braun B, Dorgan JR (2009) Single-step method for the isolation and surface functionalization of cellulosic nanowhiskers. Biomacromolecules 10:334–341

Eyley S, Thielemans W (2014) Surface modification of cellulose nanocrystals. Nanoscale 6:7764–7779

Fortunati E, Luzi F, Puglia D, Petrucci R, Kenny JM, Torre L (2015) Processing of PLA nanocomposites with cellulose nanocrystals extracted from Posidonia oceanica waste: innovative reuse of coastal plant. Ind Crops Prod 67:439–447

Goffin AL, Raquez JM, Duquesne E, Siqueira G, Habibi Y, Dufresne A, Dubois P (2011) From interfacial ring-opening polymerization to melt processing of cellulose nanowhisker-filled polylactide-based nanocomposites. Biomacromolucules 12(7):2456–2465

Goffin AL, Habibi Y, Raquez JM, Dubois P (2012) Polyester-grafted cellulose nanowhiskers: a new approach for tuning the microstructure of immiscible polyester blends. ACS Appl Mater Interfaces 4:3364–3371

Habibi Y, Goffin AL, Schiltz N, Duquesne E, Philippe Dubois P, Dufresne A (2008) Bionanocomposites based on poly(ε-caprolactone)-grafted cellulose nanocrystals by ring-opening polymerisation. J Mater Chem 18(41):5002–5010

Habibi Y, Lucia LA, Rojas OJ (2010) Cellulose nanocrystals: chemistry, self-assembly, and applications. Chem Rev 110(6):3479–3500

Haque MM, Puglia D, Fortunati E, Pracella M (2017) Effect of reactive functionalization on properties and degradability of poly(lactic acid)/poly(viny acetate) nanocomposites with cellulose nanocrystals. React Funct Polym 110:1–9

Huan S, Bai L, Liu G, Han G (2015) Electrospun nanofibrous composites of polystyrene and cellulose nanocrystals: manufacture and characterization. Rsc Adv 5:50756–50766

Jonoobi M, Harun J, Mathew AP, Oksman K (2010) Mechanical properties of cellulose nanofiber (CNF) reinforced polylactic acid (PLA) prepared by twin screw extrusion. Compos Sci Technol 70(12):1742–1747

Kamal MR, Khoshkava V (2015) Effect of cellulose nanocrystals (CNC) on rheological and mechanical properties and crystallization behavior of PLA/CNC nanocomposites. Carbohydr Polym 123:105–114

Kowalczyk M, Piorkowska E, Kulpinski P, Pracella M (2011) Mechanical and thermal properties of PLA composites with cellulose nanofibers and standard size fibers. Compos A 42:1509–1514

Lin N, Dufresne A (2013) Physical and/or chemical compatibilization of extruded cellulose nanocrystal reinforced polystyrene nanocomposites. Macromolecules 46(14):5570–5583

Lin N, Huang J, Dufresne A (2012) Preparation, properties and applications of polysaccharide nanocrystals in advanced functional nanomaterials: a review. Nanoscale 4(11):3274–3294

Liu Y, Li Y, Yang G, Zheng XT, Zhou SB (2015) Multi-stimuli responsive shape-memory polymer nanocomposite network cross-linked by cellulose nanocrystals. ACS Appl Mater Interfaces 7(7):4118–4126

Ljungberg N, Bonini C, Bortolussi F, Boisson C, Heux L, Cavaille JY (2005) New nanocomposite materials reinforced with cellulose whiskers in atactic polypropylene: effect of surface and dispersion characteristics. Biomacromolecules 6:2732–2739

Lonnberg H, Larsson K, Lindstrom T, Hult A, Malmstrom E (2011) Synthesis of polycaprolactone-grafted microfibrillated cellulose for use in novel bionanocomposites-influence of the graft length on the mechanical properties. ACS Appl Mater Interfaces 3:1426–1433

Mi HY, Jing X, Peng J, Salick MR, Peng XF, Turng LS (2014) Poly(ε-caprolactone) (PCL)/cellulose nano-crystal (CNC) nanocomposites and foams. Cellulose 21:2727–2741

Morandi G, Heath L, Thielemans W (2009) Cellulose nanocrystals grafted with polystyrene chains through surface-initiated atom transfer radical polymerization (SI-ATRP). Langmuir 25(14):8280–8286

Morelli CL, Belgacem N, Branciforti MC, Salon MCB, Bras J, Bretas RES (2016) Nanocomposites of PBAT and cellulose nanocrystals modified by in situ polymerization and melt extrusion. Polym Eng Sci 56(12):1339–1348

Nakagaito AN, Fujimura A, Sakai T, Hama Y, Yano H (2009) Production of microfibrillated cellulose (MFC)-reinforced polylactic acid (PLA) nanocomposites from sheets obtained by a papermaking-like process. Compos Sci Technol 69(7):1293–1297

Pearlman WM, Banks CK (1948) Substituted Chlorodiamino-s-triazines1. J Am Chem Soc 70(11):3726–3728

Pracella M, Haque MM, Puglia D (2014) Morphology and properties tuning of PLA/cellulose nanocrystals

bionanocomposites by means of reactive functionalization and blending with PVAc. Polymer 55:3720–3728
Rasal RM, Hirt DE (2009) Toughness decrease of PLA-PHBHHx blend films upon surface-confined photopolymerization. J Biomed Mater Res Part A 88(4):1079–1086
Rasal RM, Janorkar A, Hirt DE (2010) Poly(lactic acid) modifications. Prog Polym Sci 35(3):338–356
Roman M, Winter WT (2004) Effect of sulfate groups from sulfuric acid hydrolysis on the thermal degradation behavior of bacterial cellulose. Biomacromolecules 5(5):1671–1677
Roy D, Guthrie JT, Perrier S (2005) One-pot hyperbranched polymer synthesis mediated by reversible addition fragmentation chain transfer (RAFT) polymerization. Macromolecules 38:10363–10372
Salmieri S, Islam F, Khan RA, Hossain F, Ibrahim HMM, Miao C, Hamad WY, Lacroix M (2014) Antimicrobial nanocomposite films made of poly(lactic acid)-cellulose nanocrystals (PLA-CNC) in food applications: part A-effect of nisin release on the inactivation of Listeria monocytogenes in ham. Cellulose 21:1837–1850
Shimizu M, Fukuzumi H, Saito T, Isogai A (2013) Preparation and characterization of TEMPO-oxidized cellulose nanofibrils with ammonium carboxylate groups. Int J Biol Macromol 59:99–104
Shimizu M, Saito T, Fukuzumi H, Isogai A (2014a) Hydrophobic, ductile, and transparent nanocellulose films with quaternary alkylammonium carboxylates on nanofibril surfaces. Biomacromolecules 15:4320–4325
Shimizu M, Saito T, Isogai A (2014b) Bulky quaternary alkylammonium counterions enhance the nanodispersibility of 2,2,6,6-tetramethylpiperidine-1-oxyl-oxidized cellulose in diverse solvents. Biomacromolecules 15:1904–1909
Singhvi M, Gokhale D (2013) Biomass to biodegradable polymer (PLA). Rsc Adv 3:13558–13568
Sobkowicz MJ, Braun B, Dorgan JR (2009) Decorating in green: surface esterification of carbon and cellulosic nanoparticles. Green Chem 11:680–682
Stroganov V, Al-Hussein M, Sommer J, Janke A, Zakharchenko S, Ionov L (2015) Reversible thermosensitive biodegradable polymeric actuators based on confined crystallization. Nano Lett 15(3):1786–1790
Wang C, Huang CL, Chen YC, Hwang GL, Tsai SJ (2008) Carbon nanocapsules-reinforced syndiotactic polystyrene nanocomposites: crystallization and morphological features. Polymer 49:5564–5574
Yee YY, Ching YC, Rozali S, Hashim NA, Singh R (2016) Preparation and characterization of poly(lactic acid)-based composite reinforced with oil palm empty fruit bunch fiber and nanosilica. BioResources 11(1):2269–2286
Yin YY, Tian XZ, Jiang X, Wang HB, Gao WD (2016) Modification of cellulose nanocrystal via SI-ATRP of styrene and the mechanism of its reinforcement of polymethylmethacrylate. Carbohydr Polym 142:206–212
Yu T, Ren J, Li S, Yuan H, Li Y (2010) Effect of fiber surface-treatments on the properties of poly(lactic acid)/ramie composites. Compos Part A 41(4):499–505
Zhang NC, Yu A, Liang A, Zhang RB, Xue F, Ding E (2013) Preparation of SiC whisker and application in reinforce of polystyrene resin composite materials. J Appl Polym Sci 130:579–586
Zhang CM, Salick MR, Cordie TM, Ellingham TK, Dan Y, Turng LS (2015) Incorporation of poly(ethylene glycol) grafted cellulose nanocrystals in poly(lactic acid) electrospun nanocomposite fibers as potential scaffolds for bone tissue engineering. Mater Sci Eng C 49(39):463–471
Zoppe JO, Peresin MS, Habibi Y, Venditti RA, Rojas OJ (2009) Reinforcing poly(epsilon-caprolactone) nanofibers with cellulose nanocrystals. ACS Appl Mater Interfaces 9:1996–2004